Scattering cross sections and collision integrals for N(⁴S)–N⁺(³P) and N(⁴S)–N⁺(¹D) interactions FREE

Zi Ding (丁子) ; Zhi Qin (秦智) ✉ ; Marcin Buchowiecki ; Linhua Liu (刘林华)

Check for updates

CrossMark

View Online

Export Citation

Articles You May Be Interested In

Collision integrals for N(^{4}S)–N(^{4}S), N(^{4}S)–N(^{2}D), and N(^{4}S)–N(^{2}P) interactions

Physics of Fluids (February 2023)

Comment on "Feynman's wobbling plate," by Slavomir Tuleja, Boris Gazovic, Alexander Tomori, and Jozef Hanc [Am. J. Phys.   75 (3), 240 – 244 (2007)]

American Journal of Physics (December 2008)

First-principles binary diffusion coefficients for H, H$_2$, and four normal alkanes + N$_2$

J. Chem. Phys. (September 2014)

Scattering cross sections and collision integrals for N(^{4}S)–N$^+$(^{3}P) and N(^{4}S)–N$^+$(^{1}D) interactions

Zi Ding (丁子),[1,2] (iD) Zhi Qin (秦智),[1,2,a] (iD) Marcin Buchowiecki,[3] (iD) and Linhua Liu (刘林华)[1,2,4,b] (iD)

AFFILIATIONS

[1]Optics & Thermal Radiation Research Center, Institute of Frontier and Interdisciplinary Science, Shandong University, Qingdao 266237, China
[2]School of Energy and Power Engineering, Shandong University, Jinan 250061, China
[3]Institute of Physics, University of Szczecin, Wielkopolska 15, 70-451 Szczecin, Poland
[4]School of Energy Science and Engineering, Harbin Institute of Technology, Harbin 150001, China

[a]Author to whom correspondence should be addressed: z.qin@sdu.edu.cn
[b]Electronic mail: liulinhua@sdu.edu.cn

ABSTRACT

Collisions between nitrogen (N) and nitrogen ion (N$^+$) are fundamental phenomena in the Earth and planetary atmospheres. In this work, we carried out a theoretical study of collision data for N(^{4}S)–N$^+$(^{3}P) and N(^{4}S)–N$^+$(^{1}D) interactions, including scattering cross sections and collision integrals. Potential energy curves of N$_2^+$ are obtained using the state-of-the-art *ab initio* method and then used to provide the input for calculations of resonant charge exchange and elastic cross sections. The inelastic (corresponding to the resonant charge exchange process), elastic, and total collision integrals for N(^{4}S)–N$^+$(^{3}P) and N(^{4}S)–N$^+$(^{1}D) interactions are computed at $500 - 50\,000$ K. An analysis of the collision integrals shows that the elastic collision process should not be neglected for odd-order collision interactions at low temperatures and still makes a small contribution at high temperatures. Note that this is the first time that the cross sections and collision integrals for the N(^{4}S)–N$^+$(^{1}D) interaction are calculated using *ab initio* potential energy points. The obtained cross sections and collision integrals are essential to model the transport properties of the related plasmas.

Published under an exclusive license by AIP Publishing. https://doi.org/10.1063/5.0161756

I. INTRODUCTION

Nitrogen (N) is the most abundant element in the Earth's atmosphere. The diffusion of nitrogen ion (N$^+$) in N happens in a variety of situations, such as airglow,[1] industrial production,[2] the Earth's ionosphere,[3] gas discharge,[4] and relay electric arc.[5] Specifically in the space vehicles' reentry process,[6,7] where the temperature in the front of the vehicle is high enough to completely dissociate and partially ionize the air, the primary mechanism of heat transfer is the diffusive transfer of the enthalpy of ionization although the concentration of N$^+$ under this condition is relatively low.[8–10] Overall, the N–N$^+$ interaction contributes to the transport characteristics of related plasmas, in which the diffusive transfer is dominated by the resonant charge transfer process under most circumstances.

The N–N$^+$ interaction is also important in planetary atmospheres. For example, Saturn's atmosphere contains 98% nitrogen, and the nitrogen ions play an essential role in Saturn's magnetosphere.[11,12] Exploring N–N$^+$ interaction helps to understand atmospheric sputtering and the source of heavy ions in Saturn's magnetosphere.[13,14] These

interactions also help to provide information on the ionosphere of Saturn and Titan.[15,16]

In view of the importance of the N–N$^+$ interaction in the Earth's and planetary atmospheres, it has been investigated in several experimental and theoretical works.[17–25] Yaev *et al.*[17] measured the resonant charge exchange cross sections for the N(^{4}S)–N$^+$(^{3}P) interaction between 7 and 100 eV using the merging beam technique, which controlled the percentage of N^{++} in N$^+$ to be below 1%. Capitelli[18] calculated the resonant charge exchange cross sections at collision energies of 0.1, 1, 5, and 10 eV related to N(^{4}S)–N$^+$(^{3}P), N(^{4}S)–N$^+$(^{1}D), N(^{2}D)–N$^+$(^{1}D), and N(^{2}P)–N$^+$(^{3}P) interactions and provided the inelastic collision integrals at 10 000–20 000 K. Subsequently, Capitelli *et al.*[21] calculated the collision integrals for the N(^{4}S)–N$^+$(^{3}P) interaction at 250–100 000 K. Their team adopted the phenomenological method to calculate the collision integrals for the N(^{4}S)–N$^+$(^{3}P) interaction.[24] Most notably, Stallcop *et al.*[20] used a semi-classical WKB approach to compute the transport cross sections for the N(^{4}S)–N$^+$(^{3}P) interaction based on the theoretical potential energy points

modified using the Rydberg–Klein–Rees and experimental data. They calculated the collision integrals for the $N(^4S)$–$N^+(^3P)$ interaction at 250–100 000 K. Recently, Eletskii et al.[22] estimated the resonant charge exchange cross sections for the $N(^2D)$–$N^+(^3P)$ interaction using the asymptotic approach at collision energies of 0.1, 1, and 10 eV. Kosarim et al.[23] calculated the resonant charge exchange cross sections at collision energies of 0.1, 1, 5, and 10 eV for the $N(^4S)$–$N^+(^3P)$, $N(^2D)$–$N^+(^3P)$, $N(^2D)$–$N^+(^1D)$, $N(^2P)$–$N^+(^3P)$, $N(^2P)$–$N^+(^1D)$, and $N(^2P)$–$N^+(^1S)$ interactions using the asymptotic theory. Eletskii et al.[22] and Kosarim et al.[23] did not provide collision integrals for the N–N^+ interaction. Overall, most previous studies only focused on the interaction between the ground $N(^4S)$ atom and the ground $N^+(^3P)$ atom. However, there may be excited $N^+(^1D)$ ions in high-temperature plasmas, in which the $N(^4S)$–$N^+(^1D)$ interaction should be considered. Laricchiuta et al.[25] calculated the collision integrals for $N(^4S)$–$N^+(^1D)$ interaction considering the $^5\Pi_g$, $^5\Delta_g$, $^4\Sigma_u^-$, and $^4\Delta_u$ states, while the $N(^4S)$–$N^+(^1D)$ interaction should theoretically correlate with the $1\ ^4\Sigma_g^-$, $d\ ^4\Sigma_u^-$, $2\ ^4\Pi_g$, $2\ ^4\Pi_u$, $1\ ^4\Delta_g$, and $c\ ^4\Delta_u$ states, so their calculations were questionable. Previous work[20] only considered the inelastic resonant contribution for the N–N^+ interaction by calculating the odd-order collision integrals. However, Murphy[26] pointed out that effective odd-order collision integrals should consider the combined inelastic and elastic collision contributions. Therefore, it is necessary to provide a more detailed and reliable investigation of collision integrals for the N–N^+ interaction. On the other hand, Frost et al.[2] noted that there may be multiple electronic excited states of N^+, such as $N^+(^3P)$, $N^+(^1D)$, $N^+(^1S)$, and $N^+(^1P)$ states in the plasmas of industrial processes, such as reactive ion etching or thin-film plasmas. In state-to-state modeling plasma flows of the vehicle entry into the Earth's atmosphere, Bultel and Annaloro[27] considered several electronic states of N^+, such as $^3P_0$, $^3P_1$, $^3P_2$, $^1D_2$, and $^1S_0$. According to the statistical mechanism, the lowest two electronic states of N^+, i.e., $N^+(^3P)$ and $N^+(^1D)$, are more abundant compared to the other higher electronic states of N^+ under a specific condition. Therefore, we focus on the $N(^4S)$–$N^+(^3P)$ and $N(^4S)$–$N^+(^1D)$ interactions in this work.

The quality of the potential energy curves (PECs) is crucial for accurately calculating the collision integrals.[28–30] In previous studies,[31–33] frequently used analytical potential energy functions, such as Lennard-Jones, m-6-8, Hulburt–Hirschfelder, Murrell–Sorbie, and modified Morse potentials, were often used to describe the interaction potentials based on experimental spectroscopic parameters. However, these analytical functions cannot guarantee the accuracy of potential energy curves at short- and long-internuclear distances. Buchowiecki and Szabó[28] compared the collision integrals obtained from the analytical potential energy functions and the interpolation of ab initio potential energy points. They pointed out the importance of repulsive potentials to calculate the collision integrals and reported that the analytical exponential functions to describe the repulsive potentials are not sufficient to obtain reliable collision integrals. Their results show that the discrepancies between collision integrals based on analytical potential energy functions and those determined from the interpolation of ab initio potential energy points were 3.5% for $\sigma^2\Omega^{(1,1)*}$ and 4% for $\sigma^2\Omega^{(2,2)*}$ at 5000 K. Recently, Kim et al.[34] and Kim and Jo[35] preferred using ab initio potential energy points to compute collision integrals because the state-of-the-art ab initio methods can provide theoretically reasonable potential energy points for short- and long-internuclear distances. Of course, accurately fitting ab initio potential

energy points covering a large internuclear distance by analytical functions, such as the combined-hyperbolic-inverse-power-representation (CHIPR) method[36–38] recently used in our investigation of N–N collisions,[30] can also guarantee the reasonable behaviors in the short- and long-range regions. Note that such treatment can provide the good fitting of ab initio potential energy points, but give questionable extrapolations at internuclear distances beyond ab initio points. Thus, using such a method needs sufficient ab initio potential points covering theoretically reasonable internuclear distances. Such a method can give nearly the same collision integrals as the interpolation of ab initio potential energy points, but the fitting processes for all the electronic states may cost huge time. Therefore, the interpolation of ab initio potential energy points for the $N(^4S)$–$N^+(^3P)$ and $N(^4S)$–$N^+(^1D)$ interactions is adopted to calculate the cross sections in this work.

The present work aims to provide detailed and reliable cross sections and collision integrals for $N(^4S)$–$N^+(^3P)$ and $N(^4S)$–$N^+(^1D)$ interactions. First, we report the resonant charge exchange and elastic cross sections using high-quality ab initio potential energy points. Second, we analyze the contribution of inelastic and elastic collision processes to the total collision integrals. Finally, we provide the inelastic, elastic, and total collision integrals for $N(^4S)$–$N^+(^3P)$ and $N(^4S)$–$N^+(^1D)$ interactions at $500 - 50\,000$ K.

II. METHODOLOGY
A. Quantum approaches of the collision integrals

For the inelastic collision, the resonant charge exchange is considered and its cross section can be expressed in terms of scattering phase shift η_b, which only depends on the PECs of $\{g, u\}$ pairs for the colliding particles[20,22] and is given by[39,40]

$$Q_{ex,\Lambda}(E) = \frac{\pi}{k^2} \sum_{l=0}^{\infty} (2l+1) \sin^2(\eta_l^g - \eta_l^u), \quad (1)$$

where Λ is angular momentum, k is the wave number ($k = \sqrt{2\mu E}$, μ is the reduced mass of the ion-parent-atom interaction collision system), l is the angular momentum quantum number, and η_l^g and η_l^u are phase shifts for the symmetric and antisymmetric states, respectively. The phase shift η_l can be defined by the semi-classical Wentzel–Kramers–Brillouin (WKB) approximation:[41–44]

$$\eta_l = k \left\{ \int_{r_x}^{\infty} [G(r)]^{1/2} dr - \int_b^{\infty} \left[1 - \left(\frac{l+1}{kr} \right)^2 \right]^{1/2} dr \right\}, \quad (2)$$

where the lower limit r_x of the integral is the largest root of the following equation:

$$G(r) \equiv 1 - \frac{V(r)}{E} - \frac{b^2}{r^2} = 0, \quad (3)$$

where b equals to $(l+1/2)/k$, which can be determined by the classical impact parameter. The total resonant charge exchange cross section Q_{ex} is weighted average of the resonant charge exchange cross sections of all $\{g, u\}$ pairs.[8,21,45] The weighting factors for calculation of total resonant charge exchange cross sections are listed in Table I.

The elastic collision includes the momentum transfer and viscosity-type collision processes. The momentum transfer cross section ($Q_{el}^{(1)}$), viscosity cross section ($Q_{el}^{(2)}$), and third moment cross section ($Q_{el}^{(3)}$), which can be calculated by[46,47]

$$Q_{el}^n(E) = \frac{4\pi}{k^2} \sum_{v}^{n} \sum_{l=0}^{\infty} a_{nv}^l \sin^2(\eta_{l+v} - \eta_l), \qquad (4)$$

where the values of v are odd or even according to the parity of n. The coefficients a_{nv}^l can be determined by the recursion from[20]

$$(2l+1)x^n P_l(x) = \sum_{v=-n}^{n} a_{nv}^l P_{l+v}(x), \qquad (5)$$

where $P_l(x)$ is the Legendre polynomial. The mean elastic cross section $\bar{Q}_{el}^{(n)}$ is obtained by weighting the elastic cross sections of the corresponding states.[21]

According to the Chapman–Enskog theory,[48–50] the reduced collision integrals can be calculated by

$$\sigma^2 \Omega^{(n,s)*} = \frac{F(n,s)}{2(k_B T)^{s+2}} \int_0^{\infty} e^{-E/(k_B T)} E^{s+1} \bar{Q}^{(n)}(E) dE, \qquad (6)$$

where (n, s) is the order of collision integrals, k_B is Boltzmann constant, T is the temperature, E is the collision energy, and $\bar{Q}^{(n)}(E)$ denotes the mean inelastic cross section $\bar{Q}_{in}^{(n)}$ or mean elastic cross section $\bar{Q}_{el}^{(n)}$. The mean inelastic cross section $\bar{Q}_{in}^{(n)}$ can be determined from the resonant charge exchange cross section Q_{ex},[51,52]

$$\bar{Q}_{in}^{(n)}(E) = 2Q_{ex}(E), \qquad (7)$$

where n is odd, and Dalgarno et al.[51] suggested that the result from Eq. (7) is probably valid for temperatures greater than 400 K in most cases. The scale factor $F(n,s)$ can be obtained from the following relation:[53]

$$F(n,s) = \frac{4(n+1)}{\pi(s+1)! \left[2n+1-(-1)^n\right]}. \qquad (8)$$

The total collision integrals should consider the combined contribution of inelastic and elastic collision processes for the effective odd-order collision integral, given by[26]

$$\sigma^2 \Omega_{total}^{(n,s)*} = \sqrt{\left(\sigma^2 \Omega_{in}^{(n,s)*}\right)^2 + \left(\sigma^2 \Omega_{el}^{(n,s)*}\right)^2}, \qquad (9)$$

where the subscripts in and el denote the collision integrals derived from the inelastic and elastic interactions, respectively.

This study developed a Python code to compute the cross sections and collision integrals for N–N$^+$ interactions, where the integrals

TABLE I. The weighting factors for calculation of total resonant charge exchange cross sections.

N(^{4}S)–N$^+$(^{3}P)		N(^{4}S)–N$^+$(^{1}D)	
State	Weight	State	Weight
$^2\Sigma_{g(u)}^+$	2/36	$^4\Sigma_{g(u)}^-$	4/40
$^4\Sigma_{g(u)}^+$	4/36	$^4\Pi_{g(u)}$	8/40
$^6\Sigma_{g(u)}^+$	6/36	$^4\Delta_{g(u)}$	8/40
$^2\Pi_{g(u)}$	4/36		
$^4\Pi_{g(u)}$	8/36		
$^6\Pi_{g(u)}$	12/36		

were computed using the integration module of the SciPy package.[54] We set epsrel (i.e., the relative error tolerance) equals to 0.001 and limit (i.e., an upper bound on the number of subintervals used in the adaptive algorithm) equals to 1000 in the scipy.integrate.quad module.

B. *Ab initio* calculations of potential energy curves

In this work, the MOLPRO 2015 program package[55–57] was employed to calculate the PECs of N$_2^+$ corresponding to N(^{4}S)–N$^+$(^{3}P) and N(^{4}S)–N$^+$(^{1}D) interactions. Abrams and Sherrill[58] compared the bond-breaking reactions of BH, HF, and CH$_4$ using the state-averaged complete active space self-consistent field (CASSCF), complete-active-space second-order multi-reference perturbation theory (CASPT2),[59,60] and multireference configuration interaction (MRCI) methods. They found that perturbative treatment of dynamical electron correlation was not same as effective as MRCI for small molecular systems. Celani et al.[61] studied the Cr$_2$ using the various high-level methods, including CIPT2, CASSCF, and MRCI. They demonstrated that the MRCI+Q method can provide more accurate calculations for small molecule systems with large basis set. Moreover, the MRCI method is extensively employed in the most current studies of diatomic electronic structures.[28,62,63] Our calculations use the CASSCF method, followed by the internally contracted multireference configuration interaction method, including Davidson correction (icMRCI+Q).[64] Here, we adopted the aug-cc-pV6Z (AV6Z) basis set to describe the nitrogen atom and ion.[65–67] MOLPRO cannot take advantage of the $D_{\infty h}$ symmetry, so the $D_{\infty h}$ molecules must be treated in the corresponding subgroup. For example, N$_2^+$ belongs to $D_{\infty h}$ symmetry, which will be replaced by its maximum Abelian subgroup D_{2h}. The corresponding symmetry operations for $D_{\infty h}$ and D_{2h} are $\Sigma_g^+ \to A_g$, $\Sigma_g^- \to B_{1g}$, $\Sigma_u^- \to B_{1u}$, $\Sigma_u^+ \to A_u$, $\Pi_g \to (B_{2g}, B_{3g})$, $\Pi_u \to (B_{2u}, B_{3u})$, $\Delta_g \to (A_g, B_{1g})$, and $\Delta_u \to (B_{1u}, A_u)$.

In *ab initio* calculations, four doublet, four quartet, and four sextet electronic states correlating to the N(^{4}S)–N$^+$(^{3}P) dissociation limit and 6 quartet electronic states dissociating to the N(^{4}S)–N$^+$(^{1}D) asymptote are considered, including X $^2\Sigma_g^+$, B $^2\Sigma_u^+$, D $^2\Pi_g$, A $^2\Pi_u$, 1 $^4\Sigma_g^+$, a $^4\Sigma_u^+$, b $^4\Pi_g$, f $^4\Pi_u$, 1 $^6\Sigma_g^+$, 1 $^6\Sigma_u^+$, 1 $^6\Pi_g$, 1 $^6\Pi_u$, 1 $^4\Sigma_g^-$, d $^4\Sigma_g^+$, 2 $^4\Pi_g$, 2 $^4\Pi_u$, 1 $^4\Delta_g$, and c $^4\Delta_u$. The PECs for these 18 adiabatic potential energy curves are illustrated in Fig. 1. By comparing with previous theoretical calculations,[20,22,23] our PECs cover a wider internuclear range to accurately calculate the scattering cross sections and collision integrals (see the supplementary material for details).

Since *ab initio* methods are not applicable to calculating potential energies at very short internuclear distances, the extrapolation of the potential energies is, thus, required for calculating the collision cross sections at high collision energies. First, we extrapolate the potential energy points at short internuclear distances ($R < 0.7$ Å) by

$$V(r) = x + y e^{-zr}, \qquad (10)$$

where x, y, and z are the fitting parameters. Moreover, Bender et al.[68] and Valentini et al.[69] pointed out that the accuracy of the fitting function of the potential energy points is essential for calculations of cross sections. We fit the potential energy points with cubic spline interpolation functions using scipy.interpolate.interp1d module in Python. The total root mean square errors of cubic spline interpolation functions to *ab initio* potential energy points for N(^{4}S)–N$^+$(^{3}P) and N(^{4}S)–N$^+$(^{1}D) interactions do not exceed 10^{-9} cm^{-1}.
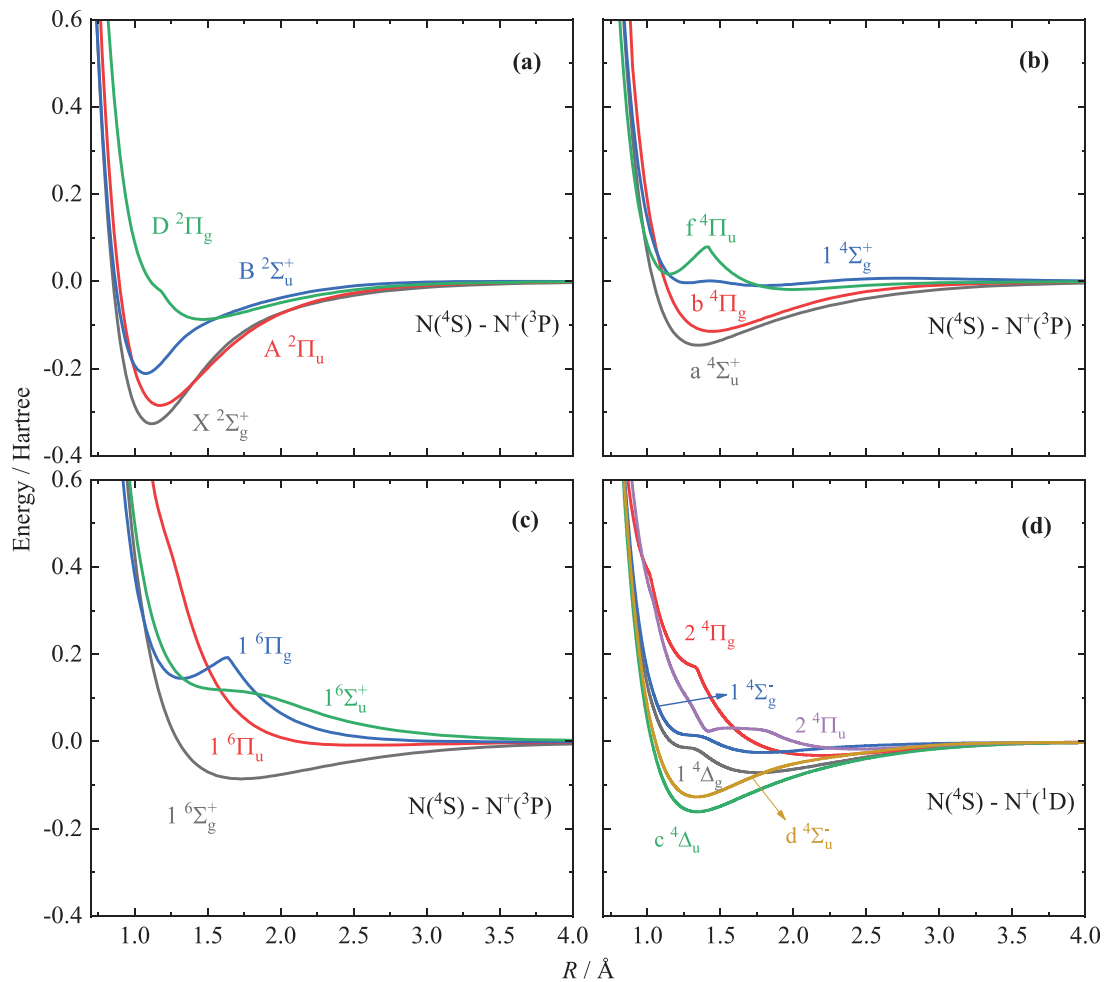
FIG. 1. Potential energy curves for the electronic states including (a) doublet states, (b) quartet states, and (c) sextet states corresponding to the N(^{4}S)–N$^+$(^{3}P) interaction, and (d) electronic states corresponding to the N(^{4}S)–N$^+$(^{1}D) interaction.

To verify the reliability of our PECs, we compared the calculated PECs of the B $^2\Sigma_g^+$ and f $^4\Pi_u$ electronic states correlating to the N(^{4}S)–N$^+$(^{3}P) interaction with those of Stallcop et al.[20] and Qin et al.,[62] as shown in Fig. 2. Stallcop et al.[20] calculated PECs at the CASSCF/GTO level. Qin et al.[62] adopted the icMRCI+Q/ACV5Z+DK level to describe the PECs of N–N$^+$ interaction. For the B $^2\Sigma_u^+$ state, our potential energy points are similar to previous theoretical ones[20] near the equilibrium structure. Our potential energy points are slightly higher than those of Stallcop et al.[20] and Qin et al.[62] for internuclear distances larger than 1.5 Å. For the f $^4\Pi_u$ state, our predicted potential energy points are slightly higher than those of Stallcop et al.[20] for internuclear distances larger than 1 Å. Our PECs match those from Qin et al.[62] for internuclear distances shorter than 1.4 Å. Our potential energy points are slightly larger than those of Qin et al.[62] for internuclear distances larger than 1.5 Å. The deviation between our PECs and those of Stallcop et al.[20] comes from the difference in basis sets. Overall, a good agreement of the B $^2\Sigma_g^+$ and f $^4\Pi_u$ states is observed,

thus confirming a good description of the *ab initio* PECs for the N–N$^+$ interaction in this work. Comparisons of our potential energy points of other electronic states with those previous calculations are given in the supplementary material.

III. ANALYSIS OF RESULTS

Figure 3 compares the resonant charge exchange cross sections for the N(^{4}S)–N$^+$(^{3}P) interaction at the collision energy of 2×10^{-4}–10 Hartree with those determined from previous theoretical calculations[18,20,22,23] and experimental measurement.[17] Our resonant charge exchange cross sections continuously oscillate as a function of collision energy, which is caused by the interference between each {g, u} pair of states for the N(^{4}S)–N$^+$(^{3}P) interaction. Particularly, our results differ greatly from those of Stallcop et al.[20] in the collision energy lower than 10^{-3} Hartree, which may be due to the difference in the PECs. The resonant charge exchange cross sections agree with the experimental values[17] within ±30%, and all within the error bars. The
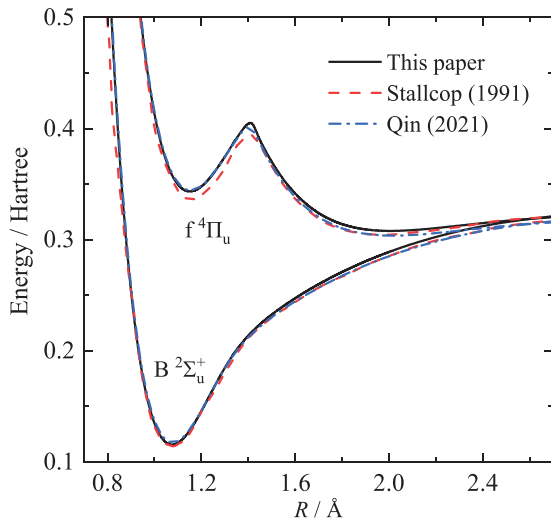
FIG. 2. Potential energy curves of the B $^2\Sigma_g^+$ and f $^4\Pi_u$ states for N$_2^+$ compared to those of Stallcop et al.[20] and Qin et al.[62]
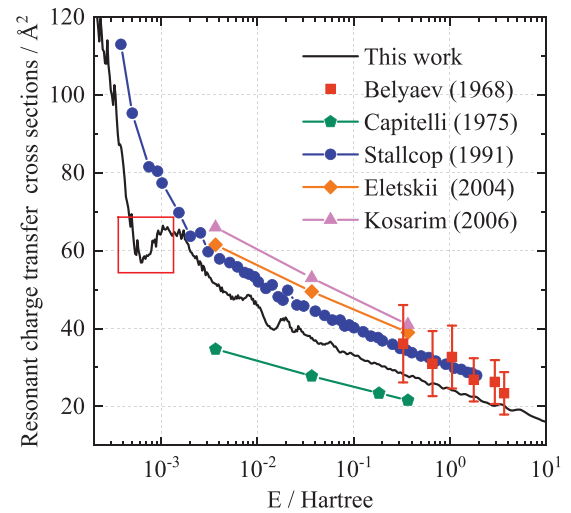

FIG. 3. Comparison of the resonant charge exchange cross sections for the N (^{4}S)–N$^+$(^{3}P) interaction as a function of collision energy, where the experimental results with error bars are from Yaev et al.[17] (squares), and the theoretical results are from Capitelli[18] (pentagons), Stallcop et al.[20] (cycles), Eletskii et al.[22] (rhombuses), and Kosarim et al.[23] (triangles), respectively.

resonant charge exchange cross sections display a large oscillatory structure at low collision energies (see the red box in Fig. 3). As pointed out by Evans and Lane,[70] the oscillatory structure is mainly caused by the scattering inside the potential barrier. Figure 3 shows that the scattering inside the potential barrier of the N(^{4}S)–N$^+$(^{3}P) interaction is approximately at a collision energy of 8×10^{-4} Hartree.

Figure 4 illustrates the mean transport cross sections $\bar{Q}_{in}^{(1)}$ and $\bar{Q}_{el}^{(2)}$ for N(^{4}S)–N$^+$(^{3}P) interaction. Stallcop et al.[20] took into account the effects of nuclear symmetry at low collision energies. They adopted twice the resonant charge exchange cross sections at high collision energies for mean transport cross sections $\bar{Q}_{in}^{(1)}$. Most studies[26,71,72] determined the inelastic cross sections by using twice the resonant

charge transfer cross sections. This work adopts the same treatment. In the other hand, Stallcop et al.[20] considered the effect of the collision energy on the contribution from each {g, u} pair of states to the mean transport cross sections. For example, the percentage contributions of $^2\Sigma_{g(u)}^+$, $^4\Sigma_{g(u)}^+$, $^6\Sigma_{g(u)}^+$, $^2\Pi_{g(u)}$, $^4\Pi_{g(u)}$, and $^6\Pi_{g(u)}$ were 7%, 15%, 25%, 7%, 7%, 18%, and 28% for the mean transport cross sections $\bar{Q}_{in}^{(1)}$ at a collision energy of 0.5 Hartree, respectively. This work adopts the same treatment of most previous studies,[8,21,45] and the weighting factors for calculating total resonant charge exchange cross sections are listed in Table I. The deviation between our predicted mean transport cross sections $\bar{Q}_{in}^{(1)}$ and those of Stallcop et al.[20] is within ±20%. Our

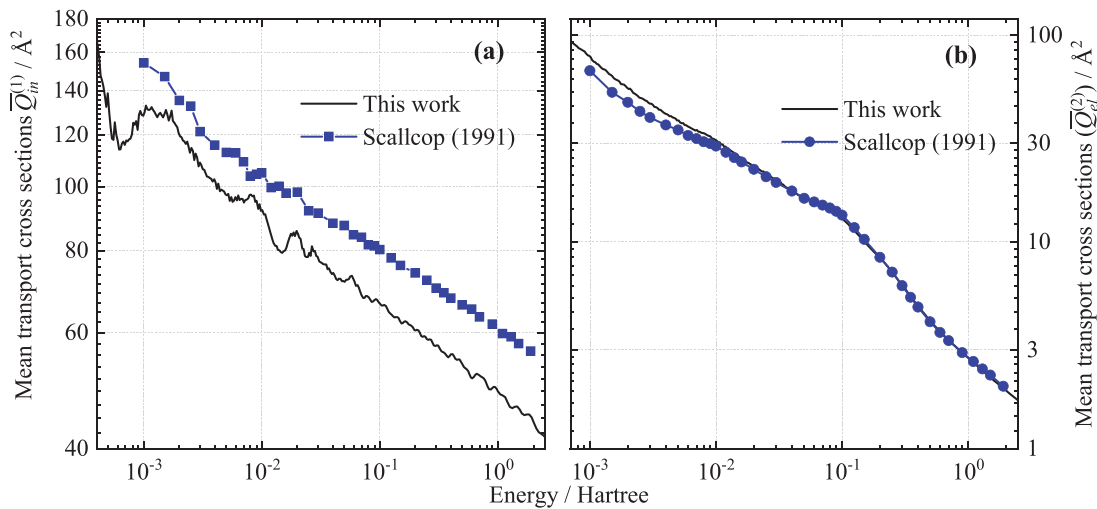**FIG. 4.** Comparison of the mean transport cross sections (a) $\bar{Q}_{in}^{(1)}$ and (b) $\bar{Q}_{el}^{(2)}$ for N(^{4}S)–N$^+$(^{3}P) collisions, where the blue symbols including squares and circles are from Stallcop et al.[20]
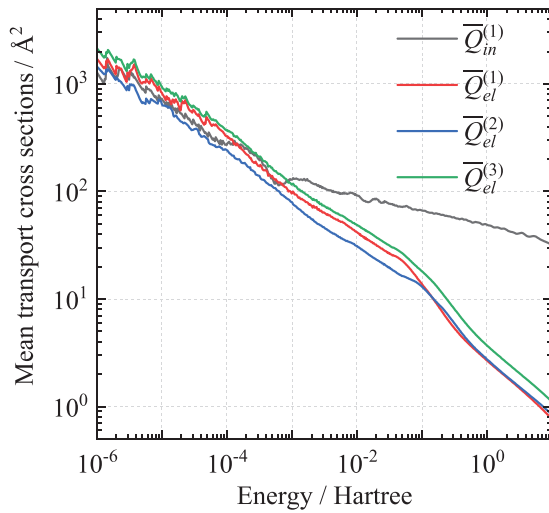
FIG. 5. The inelastic and elastic cross sections corresponding to N(^{4}S)–N$^+$(^{3}P) interaction as a function of collision energy.
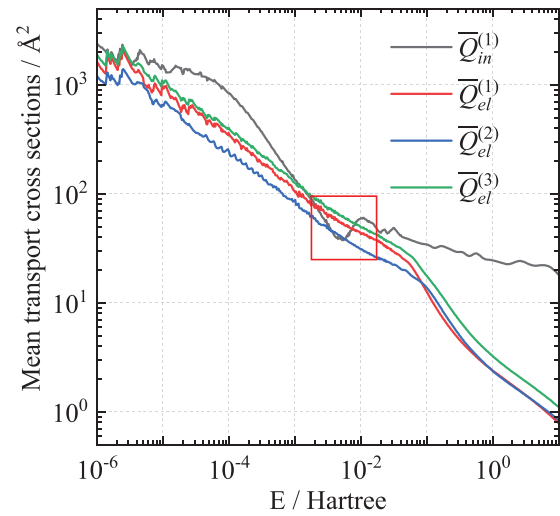

FIG. 6. The inelastic and elastic cross sections corresponding to N(^{4}S)–N$^+$(^{1}D) interaction as a function of collision energy.

viscosity cross sections $\bar{Q}_{el}^{(2)}$ are in satisfactory agreement with those of Stallcop *et al.*,[20] and the deviation is almost negligible for collision energies larger than 0.1 Hartree.

Figures 5 and 6 present the mean inelastic and elastic cross sections for N(^{4}S)–N$^+$(^{3}P) and N(^{4}S)–N$^+$(^{1}D) interactions at a wide range of collision energy. 500 and 50 points are considered in the collision energy range of 10^{-6}–1.0 Hartree and 1.0–10 Hartree, respectively. We accumulated the value of the angular momentum quantum number l to 30 000 and 10 000 for calculations of the resonant charge exchange cross sections and elastic cross sections, respectively, ensuring a decimal accuracy of five significant figures for both types of cross sections. The elastic cross sections $\bar{Q}_{el}^{(1)}$, $\bar{Q}_{el}^{(2)}$, and $\bar{Q}_{el}^{(3)}$ for N(^{4}S)−N$^+$(^{3}P) and N(^{4}S)−N$^+$(^{1}D) interactions exhibit continuous oscillations at collision energies smaller than 0.1 Hartree, due to the significant variation of partial phase shift in this collision energy region. Note that the inelastic and odd-order elastic cross sections are in the same order of magnitude at low collision energies, so the contribution of the elastic collision process should not be neglected while calculating the odd-order collision integrals.

As Cohen and Schneider[39] pointed out, the onset of excitation transfer can be much slower if the differential potential energy does not rapidly approach zero beyond the maximum potential energy. The difference of the large potential energy between the {g, u} pairs of the Δ states [see Fig. 1(d)] determines the slow decrease in inelastic cross sections for the N(^{4}S)–N$^+$(^{1}D) interaction at collision energies smaller than 10^{-4} Hartree, as shown in Fig. 6. Similarly, the {g, u} pairs of the Π states dominate the rapid decline of resonant charge exchange cross sections at collision energies of 10^{-4}–5×10^{-3} Hartree. In particular, the resonant charge transfer process begins to dominate the collision process for N(^{4}S)–N$^+$(^{3}P) and N(^{4}S)–N$^+$(^{1}D) interactions at collision energies larger than 10^{-3} and 10^{-2} Hartree, respectively.

Table II presents the comparison of inelastic collision integrals $\sigma^2\Omega_{in}^{(1,1)*}$ and elastic collision integrals $\sigma^2\Omega_{el}^{(2,2)*}$ for N(^{4}S)–N$^+$(^{3}P) interaction with the previous theoretical data,[20,21,24] respectively. For inelastic collision integrals $\sigma^2\Omega_{in}^{(1,1)*}$, our results are in better agreement with those of Stallcop *et al.*,[20] with a deviation not exceeding

TABLE II. Comparison between collision integrals $\sigma^2\Omega_{in}^{(1,1)*}$ (Å^2) for N(^{4}S)–N$^+$(^{3}P) interaction calculated in the present work (columns a), Stallcop *et al.*[20] (columns b), Capitelli *et al.*[21] (columns c) and Capitelli *et al.*[24] (columns d).

T (K)	$\sigma^2\Omega_{in}^{(1,1)*}$ (a)	$\sigma^2\Omega_{in}^{(1,1)*}$ (b)	$\sigma^2\Omega_{in}^{(1,1)*}$ (c)	$\sigma^2\Omega_{el}^{(2,2)*}$ (a)	$\sigma^2\Omega_{el}^{(2,2)*}$ (b)	$\sigma^2\Omega_{el}^{(2,2)*}$ (d)
500	33.260	38.17	⋯	18.326	16.41	13.44
1000	29.747	34.27	⋯	14.234	13.27	11.41
2000	26.890	31.39	34.5	10.904	10.50	9.54
5000	23.827	28.30	30.7	7.773	7.74	7.33
8000	22.419	26.86	⋯	6.417	6.48	6.30
10 000	21.782	26.19	28.1	5.761	5.84	5.84
15 000	20.667	25.00	26.5	4.600	4.66	5.04
20 000	19.910	24.18	25.5	3.838	3.87	4.51
50 000	17.638	21.70	22.3	2.044	2.04	⋯

TABLE III. Comparison between collision integrals $\sigma^2\Omega_{in}^{(1,1)*}$ (Å^2) for N(^{4}S)–N$^+$(^{1}D) interaction calculated in the present work (columns a) and Capitelli[18] (columns b).

T (K)	$\sigma^2\Omega_{in}^{(1,1)*}$ (a)	$\sigma^2\Omega_{in}^{(1,1)*}$ (b)
10 000	11.570	10.2
12 000	11.212	10.0
14 000	10.937	9.9
15 000	10.818	9.8
16 000	10.712	9.7
18 000	10.521	9.6
20 000	10.356	9.5

19% below 50 000 K. For viscosity collision integrals $\sigma^2\Omega_{el}^{(2,2)*}$, our results are in better agreement with those of Stallcop et al.,[20] in particular in the temperature range of 5000–50 000 K. By comparing with those obtained by the phenomenological method,[24] the maximum deviation is more than 36% at 500 K.

Table III reports the comparison of collision integrals $\sigma^2\Omega_{in}^{(1,1)*}$ for N(^{4}S)–N$^+$(^{1}D) interaction with results from Capitelli.[18] The PECs were derived from calculated by Andersen and Thulstrup[73] using the *ab initio* complete valence shell configuration interaction method. Our results are in satisfactory agreement with those of Capitelli,[18] with the percentage error not exceeding 14%.

Figure 7 displays the elastic collision integrals $\sigma^2\Omega_{el}^{(1,1)*}$, inelastic collision integrals $\sigma^2\Omega_{in}^{(1,1)*}$ and total collision integrals $\sigma^2\Omega_{total}^{(1,1)*}$ in a wide temperature range for the N(^{4}S)–N$^+$(^{3}P) interaction. The maximum contribution of the elastic collision accounts for about 13.9% of the total collision integral $\sigma^2\Omega_{total}^{(1,1)*}$ at 500 K. Moreover, it still accounts for 2.6% even at temperatures up to 10 000 K. Compared with the total collision integrals with or without the elastic collision process, the elastic collision process contribution should not be neglected for odd-order collision interactions at low temperatures and still make a small contribution at high temperatures.
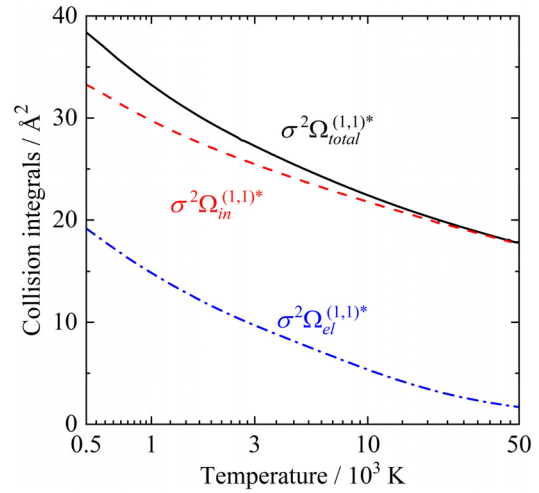

FIG. 7. The total collision integrals (solid line) corresponding to N(^{4}S)–N$^+$(^{3}P) interaction, resulting from elastic (dashed line) and resonant charge exchange (dot–dashed line) contributions.

Figures 8 and 9 illustrate the inelastic and elastic collision integrals for N(^{4}S)–N$^+$(^{3}P) and N(^{4}S)–N$^+$(^{1}D) interactions at 500–50 000 K, respectively. Note that the inelastic collision integrals for N(^{4}S)–N$^+$(^{1}D) interaction are not like the usual case of monotonically decreasing with increasing temperature at low temperatures, which may be caused by the large oscillatory structure of the inelastic collision cross sections at low collision energies, as shown in the red box in Fig. 6. At low temperatures, both the inelastic and elastic collision integrals for odd-order collision process are important for N(^{4}S)–N$^+$(^{3}P) and N(^{4}S)–N$^+$(^{1}D) interactions, while the elastic collision integrals contribute less to the total collision integral at high temperatures. Therefore, although the resonant charge transfer process plays
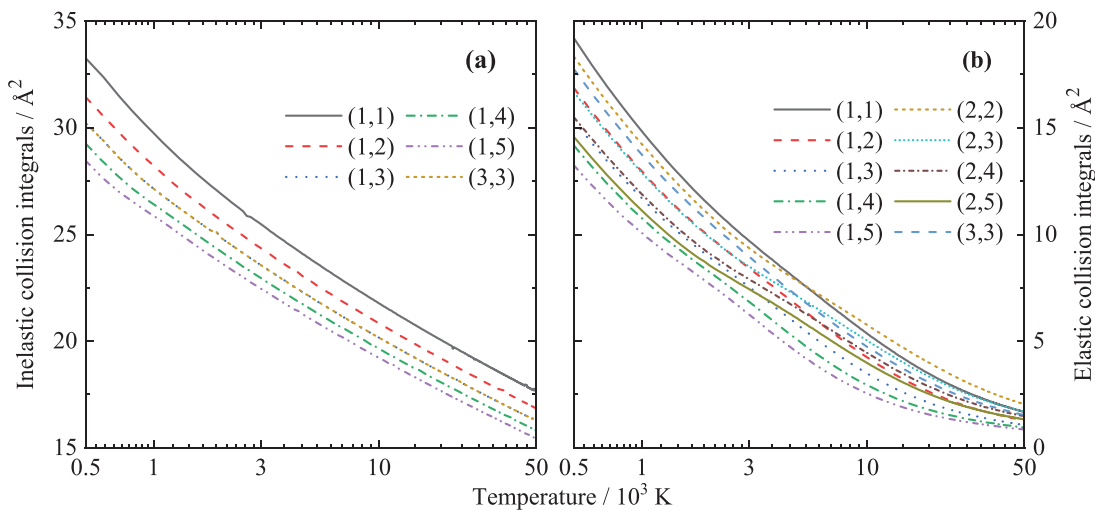

FIG. 8. (a) Inelastic and (b) elastic collision integrals corresponding to N(^{4}S)–N$^+$(^{3}P) interaction as a function of temperature.
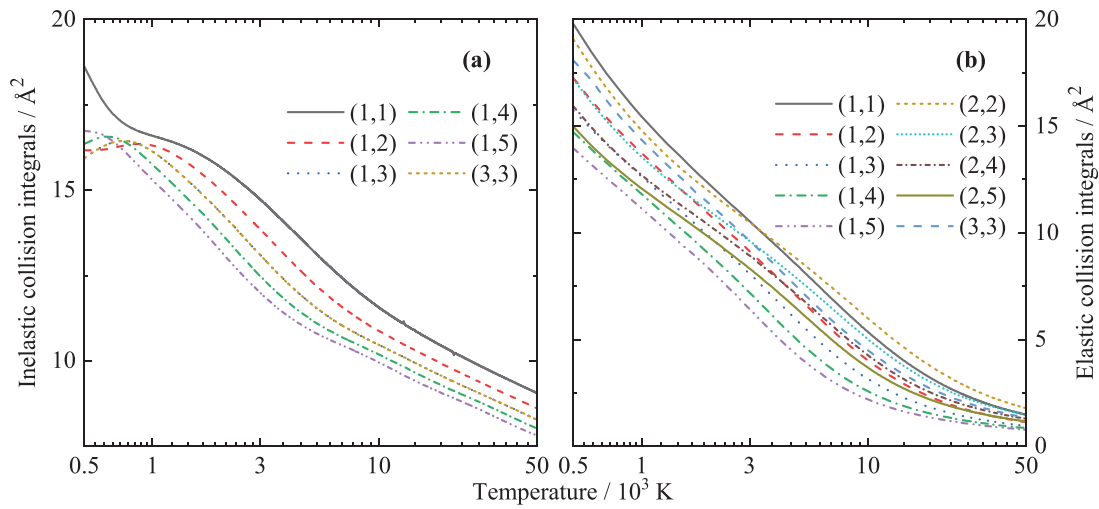
19 August 2023 02:49:20

FIG. 9. (a) Inelastic and (b) elastic collision integrals corresponding to N(^{4}S)–N$^+$(^{1}D) interaction as a function of temperature.
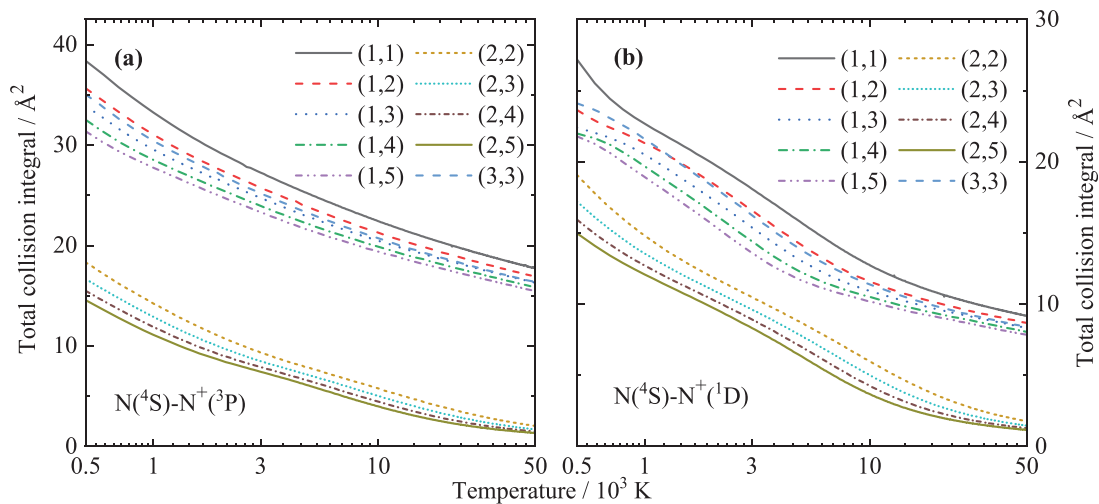

FIG. 10. The total collision integrals corresponding to the (a) N(^{4}S)–N$^+$(^{3}P) and (b) N(^{4}S)–N$^+$(^{1}D) interactions as a function of temperature.

an important role in the odd-order collision process for N–N$^+$ interaction, the combined contribution of the inelastic and elastic collision process needs to be simultaneously considered for accurately calculating the total collision integrals. Figure 10 shows the total collision integrals for N(^{4}S)–N$^+$(^{3}P) and N(^{4}S)–N$^+$(^{1}D) interactions at 500–50 000 K. The details of the inelastic, elastic, and total collision integrals are available in the supplementary material.

IV. CONCLUSIONS

In this work, we have presented a theoretical study of scattering cross sections and collision integrals for N(^{4}S)–N$^+$(^{3}P) and N(^{4}S)–N$^+$(^{1}D) interactions in the framework of the semi-classical approach based on *ab initio* potential energy points of N$_2^+$. In particular, we consider the collision energies up to 10 Hartree and the combined

contribution of inelastic and elastic collision processes for collision integrals. The results show that the elastic collision process should be considered in determining the odd-order collision integrals, especially at low temperatures. Finally, the inelastic, elastic, and total collision integrals for N(^{4}S)–N$^+$(^{3}P) and N(^{4}S)–N$^+$(^{1}D) interactions are obtained for temperatures ranging from 500 to 50 000 K and these data have potential significance for modeling the transport properties in air plasmas and planetary atmospheres.

SUPPLEMENTARY MATERIAL

The supplementary material includes comparisons of our potential energy points for N(^{4}S)–N$^+$(^{3}P) interaction with those from previous calculations given in Comparison.pdf, the *ab initio* potential energy points given in *ab initio* potential energies.txt, inelastic, elastic,

and total collision integrals for N(^{4}S)–N$^+$(^{3}P) and N(^{4}S)–N(^{1}D) interactions given in N(^{4}S)–N$^+$(^{3}P) elastic collision integrals.txt, N(^{4}S)–N$^+$(^{3}P) inelastic collision integrals.txt, N(^{4}S)–N$^+$(^{3}P) total collision integrals.txt, N(^{4}S)–N(^{1}D) elastic collision integrals.txt, N(^{4}S)–N(^{1}D) inelastic collision integrals.txt, and N(^{4}S)–N(^{1}D) total collision integrals.txt.

AUTHOR DECLARATIONS
Conflict of Interest

The authors have no conflicts to disclose.

Author Contributions

Zi Ding: Formal analysis (equal); Investigation (equal); Methodology (equal); Writing – original draft (equal). **Zhi Qin:** Conceptualization (equal); Funding acquisition (equal); Supervision (equal); Writing – review & editing (equal). **Marcin Buchowiecki:** Software (equal); Writing – review & editing (equal). **Linhua Liu:** Funding acquisition (equal); Supervision (equal); Writing – review & editing (equal).

DATA AVAILABILITY

The data that support the findings of this study are available within the article [and its supplementary material].

REFERENCES

[1] F. He, Y. Wei, and W. Wan, "Equatorial aurora: The aurora-like airglow in the negative magnetic anomaly," Natl. Sci. Rev. **7**, 1606 (2020).

[2] R. M. Frost, P. Awakowicz, H. P. Summers, and N. R. Badnell, "Calculated cross sections and measured rate coefficients for electron-impact excitation of neutral and singly ionized nitrogen," J. Appl. Phys. **84**, 2989 (1998).

[3] H. Lee, N. Kim, M. Lee, J. Kwon, S. H. Son, N. Bae, T. Park, S. Park, and G. Kim, "Investigation of ion collision effect on electrostatic sheath formation in weakly ionized and weakly collisional plasma," Plasma Sources Sci. Technol. **31**, 084006 (2022).

[4] A. Bogaerts, E. Neyts, R. Gijbels, and J. Van der Mullen, "Gas discharge plasmas and their applications," Spectrochim. Acta, Part B **57**, 609 (2002).

[5] G. Zhai and X. Zhou, "Study on arc generated by opening electromagnetic relay contacts in DC low-current resistive circuit with constant velocity," IEICE Trans. Electron. **E91-C**, 1233 (2008).

[6] H. Partridge, J. R. Stallcop, and E. Levin, "Transport cross sections and collision integrals for N (^{4}S^o)-O$^+$(^{4}S^o) and N$^+$(^{3}P)-O(^{3}P) interactions," Chem. Phys. Lett. **184**, 505 (1991).

[7] A. C. Tibère-Inglesse, S. D. McGuire, P. Mariotto, and C. O. Laux, "Experimental study of recombining nitrogen plasmas: II. Electronic population distributions and nonequilibrium radiation of atoms," Plasma Sources Sci. Technol. **30**, 125020 (2021).

[8] H. Knof, E. A. Mason, and J. T. Vanderslice, "Interaction energies, charge exchange cross sections, and diffusion cross sections for N$^+$–N and O$^+$–O collisions," J. Chem. Phys. **40**, 3548 (1964).

[9] M. Capitelli, C. Gorse, and P. Fauchais, "Transport coefficients of high temperature N$_2$-H$_2$ mixtures," J. Phys. France **38**, 653 (1977).

[10] S. Kawaguchi, K. Takahashi, and K. Satoh, "Electron collision cross section set for N$_2$ and electron transport in N$_2$, N$_2$/He, and N$_2$/Ar," Plasma Sources Sci. Technol. **30**, 035010 (2021).

[11] E. C. Sittler, R. E. Johnson, H. T. Smith, J. D. Richardson, S. Jurac, M. Moore, J. F. Cooper, B. H. Mauk, M. Michael, C. Paranicas, T. P. Armstrong, and B. Tsurutani, "Energetic nitrogen ions within the inner magnetosphere of Saturn," J. Geophys. Res. **111**, A09223, https://doi.org/10.1029/2004JA010509 (2006).

[12] H. T. Smith, *The Search for Nitrogen in Saturn's Magnetosphere* (University of Virginia, 2006).

[13] M. Michael, R. E. Johnson, F. Leblanc, M. Liu, J. G. Luhmann, and V. I. Shematovich, "Ejection of nitrogen from Titan's atmosphere by magnetospheric ions and pick-up ions," Icarus **175**, 263 (2005).

[14] R. E. Johnson, "Plasma-induced sputtering of an atmosphere," Space Sci. Rev. **69**, 215 (1994).

[15] J. H. Waite, Jr., R. S. Perryman, M. E. Perry, K. E. Miller, J. Bell, T. E. Cravens, C. R. Glein, J. Grimes, M. Hedman, and J. Cuzzi, "Chemical interactions between Saturn's atmosphere and its rings," Science **362**, eaat2382 (2018).

[16] A. J. Coates, "Interaction of Titan's ionosphere with Saturn's magnetosphere," Philos. Trans. R. Soc. A **367**, 773 (2009).

[17] V. A. Belyaev, B. G. Brezhnev, and E. M. Erastov, "Resonant charge transfer of low-energy carbon and nitrogen ions," Sov. Phys. JETP **27**, 924 (1968).

[18] M. Capitelli, "Charge transfer from low-lying excited states: Effects on reactive thermal conductivity," J. Plasma Phys. **14**, 365 (1975).

[19] M. Capitelli, U. T. Lamanna, C. Guidotti, and G. P. Arrighini, "The gerade-ungerade splitting of N$_2^+$ potentials: Effects on the resonant charge transfer cross sections of nitrogen atoms," Chem. Phys. **19**, 269 (1977).

[20] J. R. Stallcop, H. Partridge, and E. Levin, "Resonance charge transfer, transport cross sections, and collision integrals for N$^+$(^{3}P)–N(^{4}S^0) and O$^+$(^{4}S^0)–O(^{3}P) interactions," J. Chem. Phys. **95**, 6429 (1991).

[21] M. Capitelli, C. Gorse, S. Longo, and D. Giordano, "Collision integrals of high-temperature air species," J. Thermophys. Heat Transfer **14**, 259 (2000).

[22] A. V. Eletskii, M. Capitelli, R. Celiberto, and A. Laricchiuta, "Resonant charge exchange and relevant transport cross sections for excited states of oxygen and nitrogen atoms," Phys. Rev. A **69**, 042718 (2004).

[23] A. V. Kosarim, B. M. Smirnov, M. Capitelli, R. Celiberto, and A. Laricchiuta, "Resonant charge exchange involving electronically excited states of nitrogen atoms and ions," Phys. Rev. A **74**, 062707 (2006).

[24] M. Capitelli, D. Cappelletti, G. Colonna, C. Gorse, A. Laricchiuta, G. Liuti, S. Longo, and F. Pirani, "On the possibility of using model potentials for collision integral calculations of interest for planetary atmospheres," Chem. Phys. **338**, 62 (2007).

[25] A. Laricchiuta, F. Pirani, G. Colonna, D. Bruno, C. Gorse, R. Celiberto, and M. Capitelli, "Collision integrals for interactions involving atoms in electronically excited states," J. Phys. Chem. A **113**, 15250 (2009).

[26] A. B. Murphy, "Transport coefficients of air, argon-air, nitrogen-air, and oxygen-air plasmas," Plasma Chem. Plasma Process. **15**, 279 (1995).

[27] A. Bultel and J. Annaloro, "Elaboration of collisional–radiative models for flows related to planetary entries into the Earth and Mars atmospheres," Plasma Sources Sci. Technol. **22**, 025008 (2013).

[28] M. Buchowiecki and P. Szabó, "N–H collision integrals with study of repulsive interactions," Plasma Sources Sci. Technol. **31**, 045010 (2022).

[29] M. Buchowiecki and P. Szabó, "Collision integrals for nitrogen and hydrogen ionized gas: The exact values and assessment of approximations," Plasma Chem. Plasma Process. **43**, 449 (2023).

[30] Z. Ding, Z. Qin, and L. Liu, "Collision integrals for N(^{4}S)–N(^{4}S), N(^{4}S)–N(^{2}D), and N(^{4}S)–N(^{2}P) interactions," Phys. Fluids **35**, 027127 (2023).

[31] V. A. Petrov, O. A. Ranjbar, P. A. Zhilyaev, and A. N. Volkov, "Kinetic simulations of laser-induced plume expansion from a copper target into a vacuum or argon background gas based on *ab initio* calculation of Cu–Cu, Ar–Ar, and Ar–Cu interactions," Phys. Fluids **32**, 102010 (2020).

[32] U. Hohm, "Mutual intersection points of reduced collision integrals for Lennard–Jones (nm), Hulburt–Hirschfelder, and Tang–Toennies potential energy functions," Int. J. Thermophys. **43**, 147 (2022).

[33] T. Lim, "Application of extended-Rydberg parameters in general Morse potential functions," J. Math. Chem. **49**, 1086 (2011).

[34] J. G. Kim, S. H. Kang, and S. H. Park, "Thermochemical nonequilibrium modeling of oxygen in hypersonic air flows," Int. J. Heat Mass Transfer **148**, 119059 (2020).

19 August 2023 02:49:20

[35] J. G. Kim and S. M. Jo, "Modification of chemical-kinetic parameters for 11-air species in re-entry flows," Int. J. Heat Mass Transfer **169**, 120950 (2021).

[36] X. Li, Z. Qin, G. Chen, and L. Liu, " Reaction dynamics of C (^{3}P) + Si$_2$ (X)→ Si (^{3}P)+ SiC (X $^3\Pi$) on a global CHIPR potential energy surface of the ground state Si$_2$C (X ^{1}A$_1$))," Mon. Not. R. Astron. Soc. **522**, 3049 (2023).

[37] G. Chen, Z. Qin, J. Li, and L. Liu, "A global CHIPR potential energy surface of PH$_2$ (X ^{2}B$_1$) via extrapolation to the complete basis set limit and the dynamics of P (^{2}D)+H$_2$ (X $^1\Sigma_g{}^+$) → PH (X $^3\Sigma^-$)+H (^{2}S)," Phys. Chem. Chem. Phys. **24**, 19371 (2022).

[38] X. Li, Z. Qin, J. Li, and L. Liu, "An accurate NH$_2$ (X ^{2}A″) CHIPR potential energy surface via extrapolation to the complete basis set limit and dynamics of the N (^{2}D)+H$_2$ (X $^1\Sigma_g{}^+$) reaction," Phys. Chem. Chem. Phys. **24**, 26564 (2022).

[39] J. S. Cohen and B. Schneider, "Collisions of Ne∗(3s) and Ne$^+$ with Ne: Excitation and charge transfer, elastic scattering, and diffusion," Phys. Rev. A **11**, 884 (1975).

[40] J. Barata and C. Conde, *Calculation of Drift Velocities and Diffusion Coefficients of Xe/Sup+/Ions in Gaseous Xenon* (IEEE, 2004), pp. 497–501.

[41] S. Flügge, *Practical Quantum Mechanics* (Springer Science & Business Media, 1999).

[42] E. Levin, H. Partridge, and J. R. Stallcop, "Collision integrals and high temperature transport properties for N-N, O-O, and N-O," J. Thermophys. Heat Transfer **4**, 469 (1990).

[43] M. Capitelli, D. Bruno, and A. Laricchiuta, "Resonant charge exchange in ion-parent -atom collisions: The inelastic contribution to odd-order collision integrals," Fundam. Aspects Plasma Chem. Phys. **74**, 99 (2013).

[44] M. Capitelli, R. Celiberto, C. Gorse, A. Laricchiuta, P. Minelli, and D. Pagano, "Electronically excited states and transport properties of thermal plasmas: The reactive thermal conductivity," Phys. Rev. E **66**, 016403 (2002).

[45] M. Capitelli and R. S. Devoto, "Transport coefficients of high-temperature nitrogen," Phys. Fluids **16**, 1835 (1973).

[46] F. R. Meeks, T. J. Cleland, K. E. Hutchinson, and W. L. Taylor, "On the quantum cross sections in dilute gases," J. Chem. Phys. **100**, 3813 (1994).

[47] G. Heiche and E. A. Mason, "Ion mobilities with charge exchange," J. Chem. Phys. **53**, 4687 (1970).

[48] S. Chapman and T. G. Cowling, *The Mathematical Theory of Non-Uniform Gases: An account of the Kinetic Theory of Viscosity, Thermal Conduction and Diffusion in Gases* (Cambridge University Press, 1990).

[49] J. R. Stallcop, H. Partridge, and E. Levin, "Collision integrals for the interaction of the ions of nitrogen and oxygen in a plasma at high temperatures and pressures," Phys. Fluids B **4**, 386 (1992).

[50] J. O. Hirschfelder, C. F. Curtiss, and R. B. Bird, "Molecular theory of gases and liquids," in *Molecular Theory of Gases Liquids* (Wiley, 1964).

[51] A. Dalgarno and D. R. Bates, "The mobilities of ions in their parent gases," Philos. Trans. R. Soc., A **250**, 426 (1958).

[52] E. A. Mason, J. T. Vanderslice, and J. M. Yos, "Transport properties of high-temperature multicomponent gas mixtures," Phys. Fluids **2**, 688 (1959).

[53] E. Levin, D. W. Schwenke, J. R. Stallcop, and H. Partridge, "Comparison of semi-classical and quantum-mechanical methods for the determination of transport cross sections," Chem. Phys. Lett. **227**, 669 (1994).

[54] E. Jones, T. Oliphant, and P. Peterson, "SciPy: Open source scientific tools for Python" (2001).

[55] H. J. Werner, P. J. Knowles, G. Knizia, F. R. Manby, M. Schütz, P. Celani, W. Györffy, D. Kats, T. Korona, and R. Lindh, *MOLPRO, Version 2015.1, A Package of Ab Initio Programs* (University of Cardiff Chemistry Consultants (Uc3), Cardiff, Wales, England, 2015).

[56] H. J. Werner, P. J. Knowles, G. Knizia, F. R. Manby, and M. Schütz, "Molpro: A general-purpose quantum chemistry program package," WIREs. Comput. Mol. Sci. **2**, 242 (2012).

[57] H. Werner, P. J. Knowles, F. R. Manby, J. A. Black, K. Doll, A. Heßelmann, D. Kats, A. Köhn, T. Korona, D. A. Kreplin, Q. Ma, T. F. Mille. III, A. Mitrushchenkov, K. A. Peterson, I. Polyak, G. Rauhut, and M. Sibaev, "The Molpro quantum chemistry package," J. Chem. Phys. **152**, 144107 (2020).

[58] M. L. Abrams and C. D. Sherrill, "An assessment of the accuracy of multireference configuration interaction (MRCI) and complete-active-space second-order perturbation theory (CASPT2) for breaking bonds to hydrogen," J. Phys. Chem. A **107**, 5611 (2003).

[59] M. S. Grover, T. E. Schwartzentruber, Z. Varga, and D. G. Truhlar, "Vibrational energy transfer and collision-induced dissociation in O+O$_2$ collisions," J. Thermophys. Heat Transfer **33**, 797 (2019).

[60] P. Celani and H. Werner, "Analytical energy gradients for internally contracted second-order multireference perturbation theory," J. Chem. Phys. **119**, 5044 (2003).

[61] P. Celani, H. Stoll, H. Werner, and P. J. Knowles, "The CIPT2 method: Coupling of multi-reference configuration interaction and multi-reference perturbation theory. Application to the chromium dimer," Mol. Phys. **102**, 2369 (2004).

[62] Z. Qin, T. Bai, and L. Liu, "Radiative association of atomic and ionic nitrogen," Mon. Not. R. Astron. Soc. **507**, 2930 (2021).

[63] W. Xing, D. Shi, J. Zhang, J. Sun, and Z. Zhu, "Accurate potential energy curves, spectroscopic parameters, transition dipole moments, and transition probabilities of 21 low–lying states of the CO$^+$ cation," J. Quant. Spectrosc. Radiat. Transfer **210**, 62 (2018).

[64] P. J. Knowles and H. Werner, "An efficient method for the evaluation of coupling coefficients in configuration interaction calculations," Chem. Phys. Lett. **145**, 514 (1988).

[65] T. Van Mourik, A. K. Wilson, and T. H. Dunning, Jr., "Benchmark calculations with correlated molecular wavefunctions. XIII. Potential energy curves for He$_2$, Ne$_2$ and Ar$_2$ using correlation consistent basis sets through augmented sextuple zeta," Mol. Phys. **96**, 529 (1999).

[66] D. E. Woon and T. H. Dunning, Jr., "Gaussian basis sets for use in correlated molecular calculations. V. Core-valence basis sets for boron through neon," J. Chem. Phys. **103**, 4572 (1995).

[67] D. E. Woon and T. H. Dunning, Jr., "Gaussian basis sets for use in correlated molecular calculations. III. The atoms aluminum through argon," J. Chem. Phys. **98**, 1358 (1993).

[68] J. D. Bender, P. Valentini, I. Nompelis, Y. Paukku, Z. Varga, D. G. Truhlar, T. Schwartzentruber, and G. V. Candler, "An improved potential energy surface and multi-temperature quasiclassical trajectory calculations of N$_2$ + N$_2$ dissociation reactions," J. Chem. Phys. **143**, 054304 (2015).

[69] P. Valentini, M. S. Grover, and E. Josyula, "Constructing feed-forward artificial neural networks to fit potential energy surfaces for molecular simulation of high-temperature gas flows," Phys. Rev. E **102**, 53302 (2020).

[70] S. A. Evans and N. F. Lane, "Total and excitation-transfer cross sections for collisions between 2^3 S metastable and ground-state helium atoms," Phys. Rev. **188**, 268 (1969).

[71] A. Ieda, "Curved trajectory effect on charge-exchange collision at ionospheric temperatures," J. Geophys. Res. **127**, e2021JA029612, https://doi.org/10.1029/2021JA029612 (2022).

[72] G. D. Dhamale, S. Nath, V. L. Mathe, and S. Ghorui, "Neutral-neutral and neutral-ion collision integrals for Y$_2$O$_3$-Ar plasma system," Phys. Plasmas **24**, 63514 (2017).

[73] A. Andersen and E. W. Thulstrup, "Configuration interaction studies of the low-lying quartet states of N$_2{}^+$," J. Phys. B **6**, L211 (1973).

19 August 2023 02:49:20